Flow over a traveling wavy foil with a passively flapping flat plate

Nansheng Liu,[1] Yan Peng,[2,*] Youwen Liang,[1] and Xiyun Lu[1]

[1]*Department of Modern Mechanics, University of Science and Technology of China, Hefei, Anhui 230026, China*

[2]*Department of Mathematics and Statistics and Center for Computational Sciences, Old Dominion University, Norfolk, Virginia 23529, USA*

(Received 28 December 2011; revised manuscript received 4 April 2012; published 30 May 2012)

Flow over a traveling wavy foil with a passively flapping flat plate has been investigated using a multiblock lattice Boltzmann equation and the immersed boundary method. The foil undergoes prescribed undulations in the lateral direction and the rigid flat plate has passive motion determined by the fluid structure interaction. This simplified model is used to study the effect of the fish caudal fin and its flexibility on the locomotion of swimming animals. The flexibility of the caudal fin is modeled by a torsion spring acting about the pivot at the conjuncture of the wavy foil and the flat plate. The study reveals that the passively oscillating flat plate contributes half of the propulsive force. The flexibility, represented by the nondimensional natural frequency F, plays a very important role in the movement and propulsive force generation of the whole body. When the plate is too flexible, the drag force is observed. As the flat plate becomes more rigid, the propulsive force that is generated when the undulation is confined to last part of the wavy foil becomes larger. The steady movement occurs at $F = 5$. These results are consistent with the observations of some swimming animals in nature.

DOI: 10.1103/PhysRevE.85.056316 PACS number(s): 47.11.−j

I. INTRODUCTION

Natural selection has ensured that the mechanical systems evolved in fishes are highly efficient [1], and the understanding of their remarkable abilities requires interdisciplinary investigations including fish morphology and physiology, fish behavior and control, and fluid dynamics [2]. The mechanisms underlying propulsive force generation have been studied through exploration of the fluid dynamics surrounding the body. The challenges in fluid dynamics arise from the essential complexity of the unsteady motion of fish and related flow mechanisms including strong flow separation, complex vortex interaction, and fluid-structure interactions. Extensive investigations have been performed experimentally [3,4] and numerically [5–7]. By taking the rigid-body assumption, the flow patterns and the unsteady mechanism such as wake capture and reverse von Kármán vortex street have been studied in detail.

However, in nature, fish swimming is usually accompanied by obvious bending of the flexible body and flapping and pitching motions of flexible fins. Most fishes generate thrust by bending their bodies into a backward-moving propulsive wave that extends to their caudal fins. When the amplitude of body undulations is limited anteriorly and increases in the posterior half of the body, thrust is mainly provided by a caudal fin [1]. An estimated 15% of fish employ alternative swimming mechanisms that involve the use of their median and pectoral fins [1]. Analytical work and numerous recent experiments with the state-of-art particle image velocity (PIV) techniques [8–13] have provided a wealth of data in terms of both swimming kinematics and the wake flow field. However, the numerical investigations are relatively scarce, especially when compared with the exploding number of experimental papers dedicated to the same subject. The majority of the work to date on fish propulsion has focused on the body kinematics [14–20]. Patterns of body deformation during locomotion and their hydrodynamic effect have been well described [18,19]. Computational fluid dynamic analyses of body movement [14–17,20] have provided new insights into how body deformation generates the wake flow patterns and force production that power the movement of the body. Very few computational fluid dynamic approaches [21] have been carried out until recently to study the exact function of the fins based upon the assumption that the fins are rigid or have prescribed deformations.

Study of architecture in the fins of aquatic animals suggest that fish fins have anisotropic flexibility and they allow certain passive deformations [2]. This property is expected to have fundamental effects on their hydrodynamic performance in generating propulsive force. How the fins and their structural flexibility affect the performance of a fish is far from being understood.

We herein develop a model to study the body-fluid interactions during undulatory swimming and analyze the mechanisms of thrust generation, especially to elucidate the role of the caudal fin and its flexion. For the fish body, we use a wavy foil, which has been widely used in two-dimensional numerical simulations, and it undergoes prescribed undulations in the lateral direction. To model the flexible caudal fin, based on the experimental observation that the fins can easily have a passive pitching motion [22], we use a flat plate that is allowed to have a passively flapping motion stimulated by a torsion spring acting about the pivot at the juncture with the fish body [23,24]. The multiblock lattice Boltzmann method [25,26] and immersed boundary method [28–30] are used to solve the flow problems. The purpose of this study is to achieve an understanding of some fundamental phenomena such as the effects of the fin and its flexibility on thrust generation, vortical structures, and their connection to animal locomotion through this simple model.

The remainder of the paper is organized as follows. In Sec. II, the physical problem and the mathematical formulation are described. In Sec. III, we give a brief introduction to the

*Author to whom correspondence should be addressed; ypeng@odu.edu

numerical methods we used, and the validation is also given in this section. Detailed results are discussed in Sec. IV. Finally, we conclude the paper with a summary in Sec. V.

II. PHYSICAL PROBLEM AND MATHEMATICAL FORMULATION

As shown in Fig. 1, the viscous flow over a streamlined flexible body undergoing prescribed undulations in the lateral direction with a passively flapping flat plate is considered. To nondimensionalize the equations, the length of the wavy foil L and the free-stream velocity U_∞ are used as the reference length and velocity, respectively. Thus the Reynolds number Re is defined as $\mathrm{Re} = \frac{U_\infty L}{\nu}$. In this study, the length of the flat plate l is $l = \frac{L}{10}$.

The nondimensional governing equations are given as

$$\nabla \cdot \boldsymbol{u} = 0, \tag{1}$$

$$\frac{\partial \boldsymbol{u}}{\partial t} + \boldsymbol{u} \cdot \nabla \boldsymbol{u} = -\frac{1}{\rho}\nabla p + \frac{1}{\mathrm{Re}}\nabla^2 \boldsymbol{u}. \tag{2}$$

A National Advisory Committee for Aeronautics (NACA) 0012 airfoil is used as the contour of the wavy foil at an equilibrium position of the undulating motion [31–34]. The midline makes a lateral oscillation in the form of a wave traveling in the streamwise direction, and the nondimensional position is described by

$$y(x,t) = A_m(x)\cos\left[2\pi\frac{L}{\lambda}(x - ct)\right], \quad 0 \leqslant x \leqslant 1, \tag{3}$$

where A_m is the amplitude and c is the phase speed.

To model the lateral motion of the backbone undulation during swimming, the amplitude A_m is approximated by a quadratic polynomial,

$$A_m(x) = C_0 + C_1 x + C_2 x^2, \tag{4}$$

where the coefficients C_0, C_1, and C_2 are solved from the kinematic data of a steadily swimming saithe [35], which gives

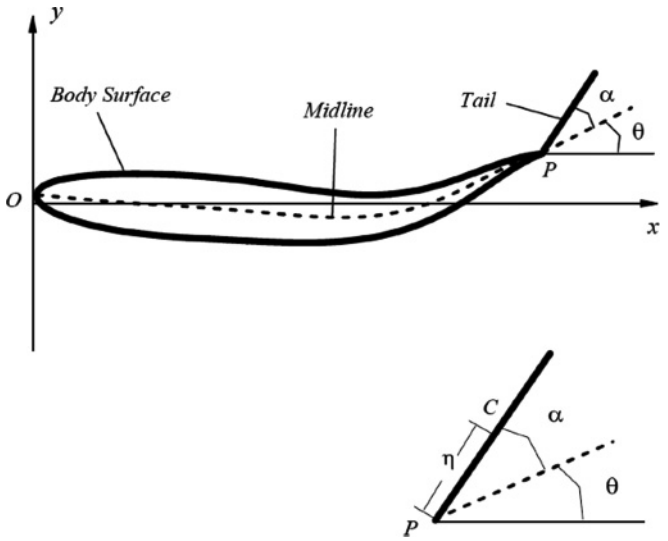

FIG. 1. Sketch of the traveling wavy foil with a passively flapping flat plate.

$A_m(0) = 0.02$, $A_m(0.2) = 0.01$, and $A_m(1) = 0.10$. Here we assume that the body undulation is a purely lateral compressive motion [5,6]. In the current study, we fix $\frac{L}{\lambda} = 1$, so that Eq. (3) simplifies to

$$y(x,t) = A_m(x)\cos[2\pi(x - ct)], \quad 0 \leqslant x \leqslant 1. \tag{5}$$

The flat plate undergoes a passive pitching motion about the point P in Fig. 1, which moves sinusoidally in the vertical direction as

$$y_p(t) = 0.1\cos(2\pi ct). \tag{6}$$

With a torsion spring acting at P, the pitching motion for the flat plate is determined by the fluid structure interaction and governed by

$$J\ddot{\alpha} + k\alpha = M_f - m\eta\cos(\theta + \alpha)\ddot{y_p} - J\ddot{\theta_p}, \tag{7}$$

where J and M_f are the moment of inertia of the flat plate and the fluid moment with respect to the point P, respectively. Additionally, k is the spring stiffness, $m = \rho_l l$ is the mass of the flat plate (ρ_l is the linear density of the plate and $\rho_l = 1/5\rho$ is used in the present study [36]), and $\eta = l/2$ is a half length of the flat plate. θ can be explicitly determined by the movement of pivot point P, which is shown in the Appendix. Consequently, Eq. (7) simplifies to the second-order ordinary differential equation in terms of α.

To describe the flexibility property of the flat plate, the natural frequency of the oscillation is introduced and defined as $f_0 = 1/2\pi\sqrt{k/J}$. The nondimensional natural frequency can be obtained as $F = Lf_0/c$ correspondingly.

III. NUMERICAL METHODS AND VALIDATION

A. Numerical methods

In this study, a multiblock lattice Boltzmann method with immersed boundary method is used. The lattice Boltzmann method is an alternative method to solve fluid dynamics problems. It has high computational efficiency and low numerical dissipation [37,38]. The immersed boundary method is used to deal with the moving boundaries, due to its easy implementation [30]. In order to obtain accurate results and reduce the computational effort, a multiblock technique is used [25,26,39,40].

1. The lattice Boltzmann equation

The lattice Boltzmann equation (LBE) with multiple-relaxation-time collision model is written as [41–43]

$$\begin{aligned}&\mathbf{f}(\boldsymbol{x}_j + \boldsymbol{c}\delta_t, t_n + \delta_t) - \mathbf{f}(\boldsymbol{x}_j, t_n)\\ &\quad = -\mathsf{M}^{-1}\cdot\hat{\mathsf{S}}\cdot[\mathbf{m}(\boldsymbol{x}_j, t_n) - \mathbf{m}^{(\mathrm{eq})}(\boldsymbol{x}_j, t_n)],\end{aligned} \tag{8}$$

where the bold-font symbols denote Q-tuple vectors, and Q is the total number of discrete velocities:

$$\begin{aligned}&\mathbf{f}(\boldsymbol{x}_j + \boldsymbol{c}\delta_t, t_n + \delta_t)\\ &\quad = (f_0(\boldsymbol{x}_j, t_n + \delta_t), f_1(\boldsymbol{x}_j + \boldsymbol{c}_1\delta_t, t_n + \delta_t),\\ &\qquad \ldots, f_b(\boldsymbol{x}_j + \boldsymbol{c}_b\delta_t, t_n + \delta_t))^{\mathsf{T}},\\ &\mathbf{f}(\boldsymbol{x}_j, t_n) = (f_0(\boldsymbol{x}_j, t_n), f_1(\boldsymbol{x}_j, t_n), \ldots, f_b(\boldsymbol{x}_j, t_n))^{\mathsf{T}},\end{aligned}$$

$b = (Q - 1)$ is the number of nonzero discrete velocities, and $\mathbf{f}$, $\mathbf{m}$, and $\mathbf{m}^{(\mathrm{eq})}$ represent the vectors whose components

are the distribution functions, the velocity moments, and the equilibrium moments, respectively. The $Q \times Q$ matrix M maps $\mathbf{f}$ to $\mathbf{m}$, that is,

$$\mathbf{m} = \mathsf{M} \cdot \mathbf{f}, \quad \mathbf{f} = \mathsf{M}^{-1} \cdot \mathbf{m},$$

and $\hat{\mathsf{S}}$ is a $Q \times Q$ diagonal matrix of the relaxation rates $\{s_i | 0 < s_i < 2\}$, that is,

$$\hat{\mathsf{S}} = \mathrm{diag}(s_0, s_1, \ldots, s_b).$$

In this work, we use the nine-velocity model in two dimensions (D2Q9 model). The discrete velocities are $\boldsymbol{c}_0 = (0,0)$, $\boldsymbol{c}_1 = (1,0)c$, $\boldsymbol{c}_2 = (0,1)c$, $\boldsymbol{c}_3 = (-1,0)c$, $\boldsymbol{c}_4 = (0,-1)c$, $\boldsymbol{c}_5 = (1,1)c$, $\boldsymbol{c}_6 = (-1,1)c$, $\boldsymbol{c}_7 = (-1,-1)c$, and $\boldsymbol{c}_8 = (1,-1)c$, where $c := \delta_x/\delta_t$. Corresponding to the nine discrete velocities $\{c_i\}$, there are nine moments:

$$\mathbf{m} = (\delta\rho, e, \varepsilon, j_x, q_x, j_y, q_y, p_{xx}, p_{xy})^{\mathsf{T}}. \tag{9}$$

The equilibria of the conserved moments, the density fluctuation $\delta\rho$ and the momentum $\boldsymbol{j} := (j_x, j_y)$, are themselves, while the equilibria of the nonconserved moments, $e, \varepsilon, \boldsymbol{q} = (q_x, q_y)$, p_{xx}, and p_{xy}, are functions of the conserved ones. With the low-Mach-number approximation, we use the following equilibria for the nonconserved moments:

$$e^{(\mathrm{eq})} = -2\delta\rho + 3\boldsymbol{j}\cdot\boldsymbol{j}, \quad \varepsilon^{(\mathrm{eq})} = \delta\rho - 3\boldsymbol{j}\cdot\boldsymbol{j}, \tag{10a}$$

$$q_x^{(\mathrm{eq})} = -j_x, \quad q_y^{(\mathrm{eq})} = -j_y, \tag{10b}$$

$$p_{xx}^{(\mathrm{eq})} = j_x^2 - j_y^2, \quad p_{xy}^{(\mathrm{eq})} = j_x j_y. \tag{10c}$$

With the orderings of the discrete velocities $\{\boldsymbol{c}_i\}$ and the corresponding moments $\{m_i\}$ given above, the transform matrix M in Eq. (8) is

$$\mathsf{M} = \begin{pmatrix} 1 & 1 & 1 & 1 & 1 & 1 & 1 & 1 & 1 \\ -4 & -1 & -1 & -1 & -1 & 2 & 2 & 2 & 2 \\ 4 & -2 & -2 & -2 & -2 & 1 & 1 & 1 & 1 \\ 0 & 1 & 0 & -1 & 0 & 1 & -1 & -1 & 1 \\ 0 & -2 & 0 & 2 & 0 & 1 & -1 & -1 & 1 \\ 0 & 0 & 1 & 0 & -1 & 1 & 1 & -1 & -1 \\ 0 & 0 & -2 & 0 & 2 & 1 & 1 & -1 & -1 \\ 0 & 1 & -1 & 1 & -1 & 0 & 0 & 0 & 0 \\ 0 & 0 & 0 & 0 & 0 & 1 & -1 & 1 & -1 \end{pmatrix}.$$

For the D2Q9 model, s_7 is determined by the shear viscosity ν [$\nu = \frac{1}{3}(\frac{1}{s_7} - \frac{1}{2})c\delta_x$] and s_1 is determined by the bulk viscosity ζ [$\zeta = \frac{1}{6}(\frac{1}{s_1} - \frac{1}{2})c\delta_x$]. It is required that $s_7 = s_8$ and $s_4 = s_6$. The relaxation rates s_0, s_3, and s_5 for the conserved moments ($\delta\rho$, j_x, and j_y) have no effect for the model, while the other relaxation rates, s_2 (for ε) and $s_4 = s_6$ (for q_x and q_y) do not affect the hydrodynamics in the lowest order approximation and only affect the small-scale behavior of the model. Usually, the values of s_2 and $s_4 = s_6$ are determined by the linear stability analysis. We use $s_2 = 1.54$ and $s_4 = s_6 = 1.9$ in the present study.

2. *The immersed boundary method*

For the two-dimensional domain Ω containing a one-dimensional closed boundary Γ, the configuration of Γ can be represented in the parametric form of $\boldsymbol{X}(\varsigma,t)$ for $0 \leqslant \varsigma \leqslant 1$, and $\boldsymbol{X}(0,t) = \boldsymbol{X}(N_\varsigma,t)$, where the parameter ς tracks a material point of the boundary. The equation of motion for a Lagrangian point on the boundary is

$$\partial_t \boldsymbol{X}(\varsigma,t) = \boldsymbol{u}(\boldsymbol{X}(\varsigma,t)) = \int_\Omega \boldsymbol{u}(\boldsymbol{x},t)\delta(\boldsymbol{x} - \boldsymbol{X}(\varsigma,t))\, d\boldsymbol{x}, \tag{11}$$

where $\boldsymbol{u}(\boldsymbol{X}(\varsigma,t))$ is the velocity of the marker at position $\boldsymbol{X}(\varsigma,t)$. By virtue of the no-slip boundary conditions, the velocity $\boldsymbol{u}(\boldsymbol{x},t)$ must also satisfy the incompressible Navier-Stokes equations:

$$\rho\partial_t \boldsymbol{u} + \rho\boldsymbol{u}\cdot\nabla\boldsymbol{u} = -\nabla p + \rho\nu\nabla^2\boldsymbol{u} + \boldsymbol{f}, \tag{12}$$

where the flow velocity $\boldsymbol{u}$, the pressure p, and the body force $\boldsymbol{f}$ evolve on the Eulerian coordinate system $\boldsymbol{x}$. The body force $\boldsymbol{f}$ is related to the boundary force $\boldsymbol{F}$ evolves on the Lagrangian coordinate system $\boldsymbol{X}$ defined by the boundary Γ as the following:

$$\boldsymbol{f}(\boldsymbol{x},t) = \int_\Gamma \boldsymbol{F}(\varsigma,t)\delta(\boldsymbol{x} - \boldsymbol{X}(\varsigma,t))\, d\varsigma, \tag{13a}$$

$$\boldsymbol{F}(\varsigma,t) = \boldsymbol{F}(\boldsymbol{X}(\varsigma,t),t). \tag{13b}$$

The essence of the immersed boundary method (IBM) is represented by Eqs. (11), (13a), and (13b). The Lagrangian markers are evolved by the velocity $\boldsymbol{u}$ and the velocity field $\boldsymbol{u}(\boldsymbol{x},t)$ must be interpolated from the Eulerian coordinate $\boldsymbol{x}$ in the flow domain Ω to the Lagrangian coordinate $\boldsymbol{X}(\varsigma,t)$ at the boundary Γ, as indicated by the integral over the flow domain Ω in Eq. (11). Likewise, the boundary force $\boldsymbol{F}$ has to be distributed from the Lagrangian coordinate $\boldsymbol{X}$ to the Eulerian one $\boldsymbol{x}$, as indicated by the integral over the boundary Γ in Eq. (13a). Obviously, the connection between the Eulerian mesh for flows and the Lagrangian markers for the boundaries relies on the approximation of the Dirac δ function. We use the following smooth approximation of the Dirac δ function in d dimensions:

$$\delta_h(\boldsymbol{x}) = \delta_h(x_1)\delta_h(x_2)\cdots\delta_h(x_d), \quad \boldsymbol{x} \in \mathbb{R}^d, \tag{14a}$$

$$\delta_h(x) = \begin{cases} \frac{1}{4h}\left[1 + \cos\left(\frac{\pi x}{2h}\right)\right] & |x| \leqslant 2h, \\ 0 & |x| > 2h. \end{cases} \tag{14b}$$

In this study, the boundary for the fish body is determined by the prescribed motion rather than solving the coupled fluid-structure interaction problem as developed by Peskin [27], so the body force $\boldsymbol{f}$ is derived by the direct forcing method [28–30], which can be written as

$$\boldsymbol{f}(\boldsymbol{x}_j) = \sum_{\boldsymbol{X}_k \in \Omega_h(\boldsymbol{x}_j)} \boldsymbol{f}'(\boldsymbol{X}_k)\delta_h(\boldsymbol{x}_j - \boldsymbol{X}_k)l_k, \tag{15}$$

where l_k is the length of boundary line segment and

$$\boldsymbol{f}'(\boldsymbol{X}) = \rho^{(n)}\left(\frac{\boldsymbol{U} - \boldsymbol{u}^{(n)}}{\delta_t} + \boldsymbol{u}^{(n)}\cdot\nabla\boldsymbol{u}^{(n)}\right) + \nabla p^{(n)} - \rho^{(n)}\nu\nabla^2\boldsymbol{u}^{(n)}. \tag{16}$$

Because the flow fields $\boldsymbol{u}$ and p are computed on the Eulerian grids $\{\boldsymbol{x}_j\}$, we use the δ function to obtain their values at a given boundary point $\boldsymbol{X}$. The detailed derivation and calculation can

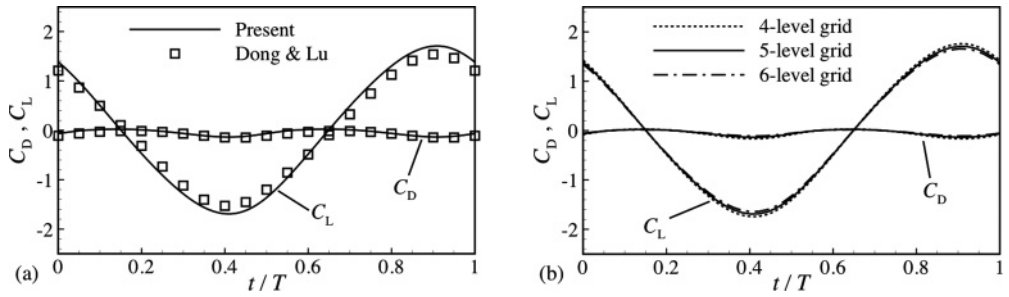

FIG. 2. Comparison of the time-dependent force coefficients of flow over a traveling wavy foil with previous study (a) and using different grid levels (b).

be found in Ref. [30]. To ensure the mass conservation up to the second-order Chapman-Enskog expansion, we include the body force f in the LBE according to the procedure found in Ref. [30].

3. The multiblock technique

We use the multiblock technique proposed by Yu [25], and the details of its application to the multiple-relaxation-time collision can be found in Ref. [26]. The coarse block boundary is in the interior of the fine block, and the fine block boundary is in the interior of the coarse block. Velocity, density, and stress are continuous across the interface. The three-point Lagrangian formulation is used for the temporal interpolation at the interface. In the present study, a five-level grid is used. The coarsest grid level has the spatial step size of $0.02L$. Because the spatial step size ratio from coarse grid to fine grid is 2, the spatial step size on the finest grid is $L/800$. In the context of the multiblock lattice Boltzmann method, the nondimensional time step size is 0.02 at the coarsest grid level and $1/800$ at the finest grid level.

B. Validation

To validate our code, we have carried out extensive simulations of the flow over a single traveling wavy foil (without a flat plate) and compared them with the published results using the space-time finite element method [33]. One typical example with $\mathrm{Re} = 5000$ and $c = 2.0$ using a five-level grid is shown here in Fig. 2(a). We compared the time-dependent drag and lateral force coefficients during one cycle for flow over a single traveling wavy foil and found that the results agree well. The maximum percentage differences are approximately 5% and 7% for the drag and lateral force coefficients respectively. To confirm grid independence, we also carried out the simulations using the four-level and six-level grids, for which the finest grid sizes are $L/400$ and $L/1600$ respectively. The time-dependent force coefficients are shown in Fig. 2(b). We can see that a five-level computational grid is fine enough to resolve the fluid dynamics in this study.

IV. NUMERICAL RESULTS AND DISCUSSIONS

In this section, we present some results of the dynamic behaviors and propulsive properties of the passively pitching plate due to the fluid-structure interaction. The effects of the flexibility of the flat plate are presented and analyzed. Motivated by the measurements of animal locomotion, the parameters considered are the phase speed of traveling wave $c = 1.2, 1.5$, and 2.0, and Reynolds number $\mathrm{Re} = 5000$. Based on the measurements of Bainbridge [36], Zhang *et al.* [44] estimated that the nondimensional natural frequency, which reflects the stiffness for the caudal fin, is about 2–6 for the tail fin of goldfish *Carassius auratus*. So in this study, F is selected as $F = 0.5$, 5, 8, and 10, which varies close to the estimated value of 2–6. The domain size is $[-12, 30]$ in the x direction and $[-12, 12]$ in the y direction. The position of the starting point of the traveling wavy foil is at (0,0) and it takes prescribed undulations in the lateral direction. So the uniform flow U_∞ is used as the inflow condition. This is similar to the experiment carried out by Lauder *et al.* [45], in which the swimming fish is held behind the head to allow only the imposition of heave and pitch motions. Extrapolation is used as the outflow condition.

A. Effect of flexibility of passively oscillated flat plate on forces and power consumption

Since the phase speed of traveling wave is a key parameter for the propulsion of the undulating body, we take it into consideration when we study the effect of the flexibility of the flat plate. We investigate the drag force acting on the wavy foil with a flat plate, the power needed, and the efficiency of the propeller when it generates the net thrust, all of which are relevant to the study of fish locomotion. Their definitions are as follows:

The total drag force on the fish consists of a friction drag and a form drag due to the pressure distribution. The corresponding drag coefficient is defined as

$$C_D = \frac{F_D}{\frac{1}{2}\rho U_\infty^2 L}. \tag{17}$$

The total power required for the propulsive motion consists two parts. One is the swimming power required to produce the lateral oscillation of traveling wave motion, which is defined as

$$P_S = -\int_{SF} f_y \frac{dy_w}{dt} ds - \int_{SP} f_y \frac{dy_w}{dt} ds, \tag{18}$$

where SF is the surface of the foil, SP is the surface of the flat plate, f_y is the force per unit length on the surface of the foil, y_w is the lateral position along the surface, and ds is the length of an element on the surface. The other is the power needed to

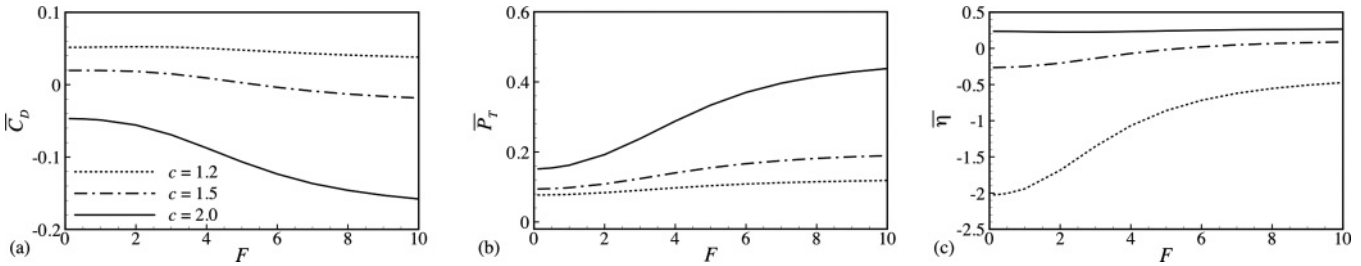

FIG. 3. Time-averaged drag force coefficient (a), power (b), and the propeller efficiency (c). Solid lines: $c = 2.0$, dashed lines: $c = 1.5$, and dotted lines: $c = 1.2$.

overcome the drag force $P_D = F_D U_\infty$. Thus the total power is obtained by $P_T = P_S + P_D$ [46,47]. The propeller efficiency is defined in a time-averaged manner as the ratio of $-\overline{P}_D$ to $\overline{P}_S$, which is $\eta = \frac{-\overline{P}_D}{\overline{P}_S}$.

Figure 3 shows the effect of F on the performance in terms of the averaged drag coefficient, the power consumed, and the propeller efficiency at different values of c. As seen from Fig. 3(a), with the increase of c, the time-averaged drag force coefficient $\overline{C}_D$ decreases for each value of F. For $c = 1.2$, $\overline{C}_D$ is always positive. For $c = 1.5$, $\overline{C}_D$ is positive for small values of F and becomes negative (acts as thrust) approximately when $F > 5.4$. The thrust force increases as F increases. From the previous study [33], it was found that without the flat plate, the drag force is always positive at $c = 1.5$ and a net thrust occurs only when c increases to 2. This observation shows the contribution of the flat plate to the thrust generation and indicates that the flexibility of flat plate has an important effect on the performance. When the flat plate is rigid enough, thrust can be generated. When it is too flexible, instead of the thrust, the drag force is generated. This finding agrees with some observations that many carangiform swimmers are capable of backward as well as forward swimming as anguilliform swimmers [1], and backward swimming requires increased lateral displacements and body flexibility [48]. For $c = 2.0$, a net thrust always occurs. The thrust force increases as F increases. Therefore higher swimming speed is expected for a fish swimmer with larger caudal fin stiffness, which is consistent with the numerical findings reported by Tytell *et al.* [49] that higher swimming speed is found for a swimming lamprey with higher stiffness for the entire body including the caudal fin. According to the previous study, the value of $\overline{C}_D$ is 0.072 without the flat plate. Adding the flat plate to the foil, the value increases to 0.16 when the flat plate is rigid enough, over two times larger than the previous value without the flat plate, which shows the influence of the flat plate. This result also agrees well with the finding that when the body undulations of the carangiform swimmers are confined to the last third of the body length, thrust is provided by a rather stiff caudal fin [1]. In our current kinetic model, the lateral motion is confined to the back of the body.

For the power consumed, as we know that $\overline{P}_S$ increases as c increases. The power to overcome the drag force $\overline{P}_D$ decreases monotonically with c, similar to the decrease of C_D, as shown in Fig. 3(a). When the wavy foil is propelled by the thrust, $\overline{P}_D$ becomes negative. However, the generation of the thrust is at the expense of the swimming power $\overline{P}_S$ required to produce the wavy foil motion [50]. The overall trend as shown in Fig. 3(b) is that power consumed increases as c increases for each F. For the same c, the more rigid the flat plate is, the more power it needs to generate the thrust. Compared to the foil without the flat plate, more power is needed to generate the motion of the flat plate.

When the undulating body is subject to a net thrust, we should consider the propeller efficiency. For $c = 1.5$, we can see from Fig. 3(c), the propeller efficiency is zero when $F = 5.4$ approximately, which agrees with Fig. 3(a) that the time-averaged net thrust force is zero. When $F > 5.4$, the propeller efficiency is around 7%. The propeller efficiency is not greatly affected by an increase of F. For $c = 2.0$, η is about 27%. This is less than the case for the foil without the flat plate, which is about 30% as reported in the previous study [50].

In order to elucidate the effect of F on the behavior of time-dependent drag, lateral forces, and power required, we calculated the root-mean-square (rms) values: $C_{D\text{rms}}$, $C_{L\text{rms}}$, and P_{rms} at different values of c and the results are shown in Fig. 4. Periodic results are obtained after five or six periods in our study. One may note that smaller rms values mean that the undulatory body would have more steady movement. We

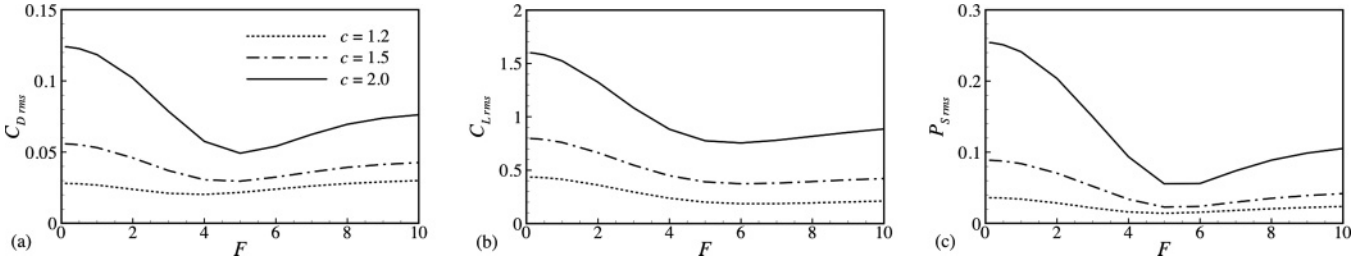

FIG. 4. Root-mean-square values of drag force (a), lateral force (b), and power (c). Solid lines: $c = 2.0$, dashed lines: $c = 1.5$, and dotted lines: $c = 1.2$.

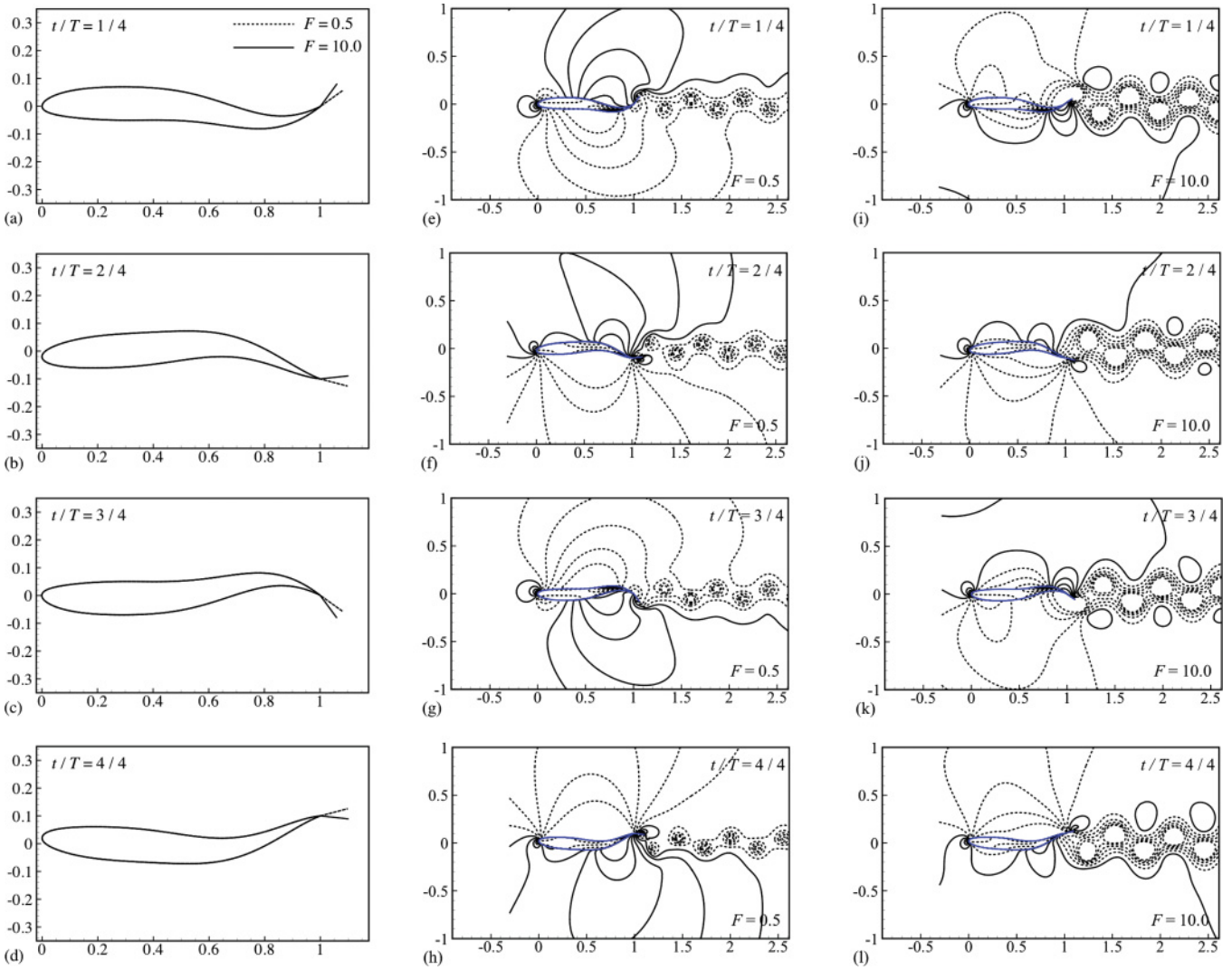

FIG. 5. (Color online) Wake foil with flapping plate in one cycle [(a)–(d)] and pressure contours $[(p - p_\infty)/\rho U_\infty^2]$ in the wake flow for $F = 0.5$ [(e)–(h)], and $F = 10$ [(i)–(l)] at $c = 2.0$. In the pressure contours, solid lines represent positive values and dashed lines represent negative values.

focus on the case $c = 2$ in which thrust can be generated. We can see that $C_{D\text{rms}}$, $C_{L\text{rms}}$, and P_{rms} decrease with F first, until they reach their minimum values at about $F = 5$. After that, they increase with F. We can conclude that the flexibility of the flat plate affects the steady movement of swimmers. For the current study, the prediction of the optimized frequency ratio $F = 5$ at $c = 2$ is in good agreement with the $F = 2$–6 measured for the goldfish's tail-fin motion [44].

B. Effect of flexibility of passively oscillated flat plate on the flow field

To study the effect of the flexibility of a passively oscillated flat plate on the flow field, we choose $c = 2$ since we know that thrust can be generated at this phase speed from Sec. IV A. A previous study [33] has found that for the traveling wavy foil, the time-dependent friction drag force is nearly constant

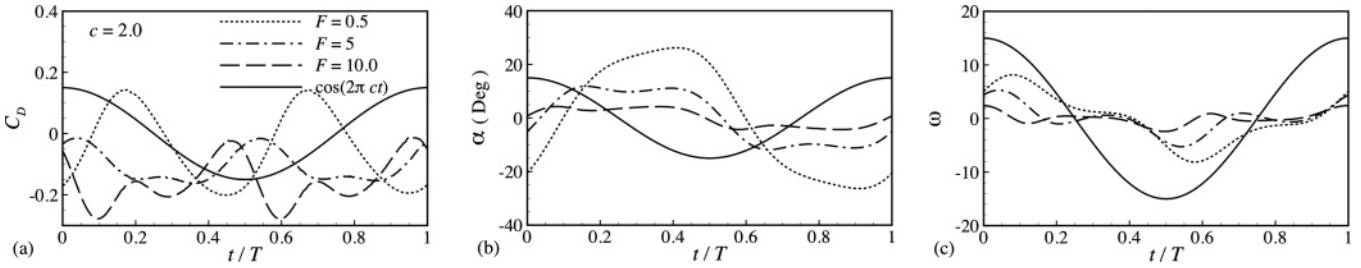

FIG. 6. Time-dependent drag coefficient (a), the angular displacement (b), and the angular velocity (c) of the flapping plate with respect to the midline movement at $c = 2.0$.

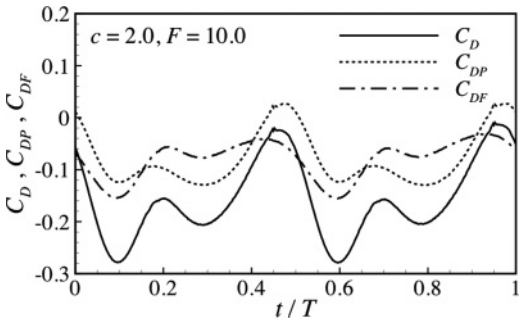

FIG. 7. Contributions of flapping plate and traveling wavy foil to the total thrust force for $c = 2.0$ and $F = 10$.

during the one cycle and that the form drag due to the pressure distribution plays an essential role in the propulsion. Figure 5 shows the pressure contours, defined as $(p - p_\infty)/\rho U_\infty^2$, in wake flow for different values of F. Solid lines represent positive values and dashed lines represent negative values. $F = 0.5$ corresponds to the very flexible flat plate, and $F = 10$ corresponds to the almost rigid flat plate.

In order to clearly see the effect of the flexibility of the flat plate, the time-dependent drag coefficient, angular displacement, and angular velocity of the flat plate with respect to the midline movement of body are also shown in Fig. 6. From Figs. 6(b) and 6(c), greater flexibility of the flat plate implies larger angular displacement and angular velocity of the flat plate with respect to the midline movement.

For the pressure field, at $t/T = 1/4$, the pivot point P starts to move downward. As seen from Figs. 6(b) and 6(c), for the more flexible flat plate with $F = 0.5$, its movement largely lags behind the movement of the midline due to its flexibility. Because of its unfavorable position relative to the wavy foil, a large positive-pressure region is formed on the top of flat plate and a lower pressure region is formed on the bottom of the flat plate, which contributes to drag force and explains why C_D in Fig. 6(a) is positive for $F = 0.5$ at this time. On the other hand, for the more rigid flat plate with $F = 10$, its movement almost has the same pace as the wavy foil. Due to its favorable relative position, a negative-pressure region is formed on the top of the flat plate and a positive-pressure region is formed on the bottom of the flat plate, which contributes to thrust force and explains why C_D in Fig. 6(a) is negative for $F = 10$. When time increases to $t/T = 2/4$, the pivot point P is at the lowest point and prepares to move upward. Due to the large flexibility of the flat plate with $F = 0.5$, it just starts to move downward with negative angular velocity. A small positive-pressure region appears at the bottom of the flat plate, which corresponds to the small thrust generated. The positive pressure becomes stronger when $t/T = 3/4$, but the angle of the flat plate is below the horizontal direction, so the total effect is the drag force. For the rigid flat plate, positive pressure appears on the top and negative pressure on the bottom, which contributes to the thrust shown in Fig. 6(a). When $t/T = 4/4$, a positive-pressure region appears at the top of the flat plate with $F = 0.5$ and a small thrust is generated.

C. Contributions of wavy foil and flat plate to the propulsion performance

To better understand the performance of a wavy foil with the passively flapping flat plate, especially regarding their separate contributions, we analyze the pressure distribution and vortex structure for one cycle. We focus on $F = 10$ and $c = 2.0$ because thrust is generated during one cycle. Figure 7 shows the contributions of the flapping plate and the traveling wavy foil to the total thrust force. In this figure, C_D is the total thrust coefficient, C_{DP} is the thrust coefficient obtained from the flat plate, and C_{DF} is the thrust coefficient calculated from the wavy foil only. We can see that both the foil and the flat plate contribute to the thrust. The contribution from the flat plate has almost the same magnitude as the foil, which explains

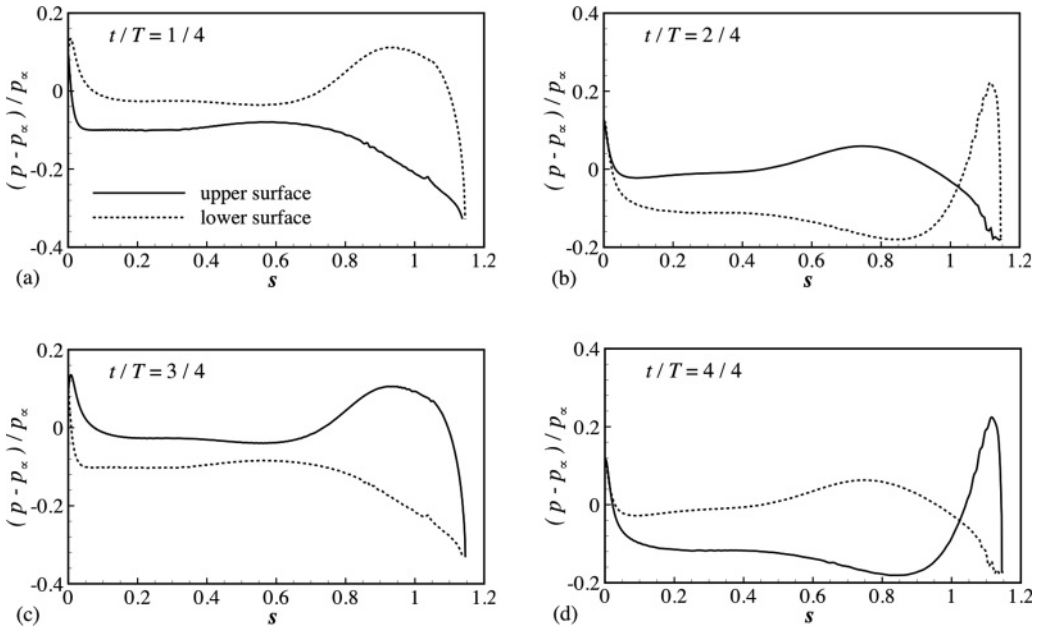

FIG. 8. Pressure distribution along the body surface during one cycle for $c = 2.0$ and $F = 10$.

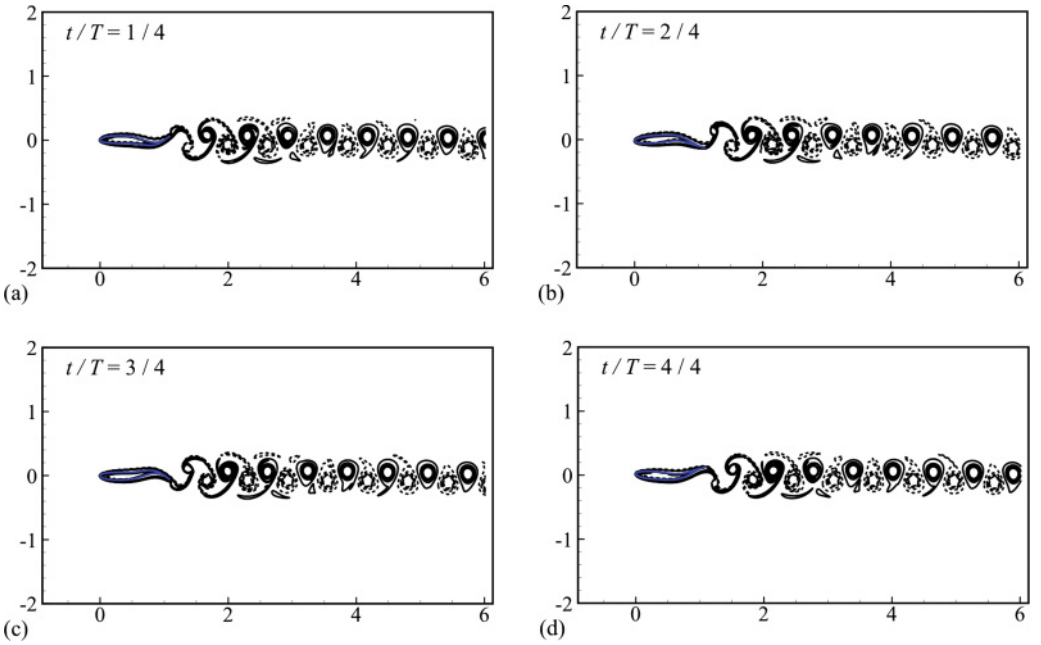

FIG. 9. (Color online) Wake vortex pattern during one cycle for $c = 2.0$ and $F = 10$. In the vortex contours, solid lines represent positive values and dashed lines represent negative values.

why the thrust doubles with the flat plate when compared with the foil without the flat plate. This also agrees with the finding that swimmers using undulation movement confined to the last third of the body length will use a rather stiff caudal fin to generate the thrust [1].

Figure 8 shows the pressure distribution along the body surface. We can see that the effective area enclosed between the pressure distribution lines on the upper and lower surfaces are largest, especially in the area formed by the pressure distribution lines on the flapping flat plate, at $t/T = 1/4$ and $3/4$, which correspond to the times of the two maximum thrusts generated in Fig. 7.

The reason why the thrust is generated and two maximum values happen at $t/T = 1/4$ and $3/4$ can be explained from the wake vortex pattern. Figure 9 shows the wake vortex pattern during one cycle. As seen from Fig. 9(a), when $t/T = 1/4$, a positive rotational vortex is formed and attached to the upside of the tail. It moves to the downwind side of the flat plate to induce a lower pressure region in the upper side of the flat plate, which can be seen in Fig. 8(a). Because the flat plate is located at a position with a positive angle with respect to the horizontal direction, the effect of the force is thrust. Also as seen from Fig. 9(a), a reverse von Kármán vortex street occurs, and it induces a jetlike mean velocity profile in the wake and also helps in the generation of thrust. When $t/T = 2/4$, as the vortex moves to the end of the tail and starts to shed into the wake, the pressure difference decreases, as seen in Fig. 8(b), and the thrust decreased. When $t/T = 3/4$, a positive rotational vortex is formed and attached to the bottom of the tail, which induces a lower pressure region in the lower side of the flat plate. Due to the negative sign of the angle of flat plate $\alpha + \theta$, the effective force is still thrust. With the shedding of the vortex at $t/T = 4/4$, the thrust decreased.

V. CONCLUSIONS

The locomotion of a traveling wavy foil with a passively flapping flat plate is studied using a multiblock lattice Boltzmann method with immersed boundary method. The wavy foil is used to model the fish body, and it undergoes prescribed undulations in the lateral direction. A flat plate is used to model the caudal fin and its flexibility is modeled by a torsion spring acting about the attachment of the fin to the body. The role of the fin and its flexibility on the propulsion performance has been studied. We briefly summarize the results obtained in this study and their relation to the real locomotion of swimming animals.

We have found that the flat plate contributes half of the thrust and that the natural frequency of the oscillating flat plate F (which indicates the flexibility of the flat plate) plays an important role in the propulsion generation. With the flat plate, thrust can be generated when $c = 1.5$ and the flat plate is not too flexible ($F > 5.4$), in contrast to the drag force without the flat plate. When the flapping plate is too flexible, drag force is generated instead of the thrust. As the flat plate becomes more rigid, the thrust it can generate becomes larger. This agrees with some findings in nature that backward swimming requires increased body flexibility and that the most thrust is provided by a rather stiff caudal fin. The magnitude of thrust with the flat plate can be two times larger than the foil without the flat plate at $c = 2.0$. We also find that with $F = 5$ at $c = 2$, the fish maintains a steady movement, which is in good agreement with $F = 2$–6 measured for the goldfishes' tail-fin motion [36].

The pressure field and vortex structure also depend on the value of F. The pressure distribution plays an essential role in the propulsion. A reverse von Kármán vortex street, which is associated with the thrust production in animal locomotion, occurs when $F > 5$ at $c = 1.5$.

The results obtained in this study may provide physical insight into the understanding of the role of the fin and its flexibility in swimming animals for propulsion generation. Ideally, it is better to explore a wide parameter space of the model (changing the value of λ/L, or the Reynolds number) to study the effect of flexibility. Also, three-dimensional computations of viscous flows around flexible bodies with more realistic fin models, such as when the entire caudal fin is allowed to be flexible, are desirable. Based on the experimental results [18], it is expected that the fluid dynamics would be similar to the current study and the magnitude of propulsive force may be increased when the entire caudal fin is flexible. These will be the subjects of our future work.

ACKNOWLEDGMENTS

This work was supported by the Natural Science Foundation of China (Grant No. 10832010, 10972211), the Innovation Project of the Chinese Academy of Sciences (Grant No. KJCX2-YW-L05) and the Innovation Foundation of the Chinese Academy of Sciences (Grant No. CXJJ-11-M69).

APPENDIX

θ can be defined as

$$\theta(t) = \tan^{-1}(Z(x,t)|_{x=1}), \tag{A1}$$

where

$$Z(x,t)|_{x=1} = \left.\frac{\partial y}{\partial x}\right|_{x=1} = (c_1 + 2c_2)\cos(2\pi ct) + 0.2\pi \sin(2\pi ct). \tag{A2}$$

Correspondingly, the derivative of θ can be obtained:

$$\dot{\theta} = \left.\frac{1}{1+Z^2}\frac{\partial Z}{\partial t}\right|_{x=1,} \tag{A3}$$

$$\ddot{\theta} = \left.\frac{1}{1+Z^2}\frac{\partial^2 Z}{\partial t^2}\right|_{x=1} - \left.\frac{2Z}{(1+Z^2)^2}\left(\frac{\partial Z}{\partial t}\right)^2\right|_{x=1,} \tag{A4}$$

so θ and its derivatives can be explicitly determined by the movement of pivot point P.

[1] M. Sfakiotakis, D. M. Lane, and J. B. C. Davies, IEEE J. Ocean Eng. **24**, 237 (1999).
[2] Q. Zhu and K. Shoele, J. Exp. Biol. **211**, 2087 (2008).
[3] R. Gopalkrishnan, M. S. Triantafyllou, G. S. Triantafyllou, and D. Barrett, J. Fluid Mech. **274**, 1 (1994).
[4] M. S. Triantafyllou, G. S. Triantafyllou, and D. K. P. Yue, Annu. Rev. Fluid Mech. **32**, 33 (2000).
[5] H. Liu, R. Wassersug, and K. Kawachi, J. Exp. Biol. **199**, 1245 (1996).
[6] H. Liu, R. Wassersug, and K. Kawachi, J. Exp. Biol. **200**, 2807 (1997).
[7] H. Liu, Appl. Mech. Rev. **58**, 269 (2005).
[8] U. K. Muller, B. L. E. Van Den Heuvel, E. J. Stamhuis, and J. J. Videler, J. Exp. Biol. **200**, 2893 (1997).
[9] U. K. Muller, E. J. Stamhuis, and J. J. Videler, J. Exp. Biol. **203**, 193 (2000).
[10] J. C. Nauen and G. V. Lauder, J. Exp. Biol. **204**, 2251 (2001).
[11] E. G. Drucker and G. V. Lauder, Integr. Comp. Biol. **42**, 243 (2002).
[12] J. C. Nauen and G. V. Lauder, J. Exp. Biol. **205**, 1709 (2002).
[13] E. D. Tytell and G. V. Lauder, J. Exp. Biol. **207**, 1825 (2004).
[14] J. Carling, T. L. Williams, and G. Bowtell, J. Exp. Biol. **201**, 3143 (1998).
[15] R. Ramamurti, R. Lohner, and W. C. Sandberg, Int. J. Comput. Fluid Dyn. **13**, 83 (1999).
[16] M. J. Wolfgang, J. M. Anderson, M. A. Grosenbaugh, D. K. Yue, and M. S. Triantafyllou, J. Exp. Biol. **202**, 2303 (1999).
[17] Q. Zhu, M. J. Wolfgang, D. K. Yue, and G. S. Triantafyllou, J. Fluid Mech. **468**, 1 (2002).
[18] F. Fish and G. V. Lauder, Annu. Rev. Fluid Mech. **38**, 193 (2006).
[19] G. V. Lauder and E. D. Tytell, Fish Biomech. **23**, 425 (2006).
[20] S. Kern and P. Koumoutsakos, J. Exp. Biol. **209**, 4841 (2006).
[21] R. Mittal, H. Dong, M. Bozkurttas, G. V. Lauder, and P. G. A. Madden, Bioinsp. Biomimet. **1**, 35 (2006).
[22] A. R. Ennos, J. Exp. Biol. **127**, 355 (1987).
[23] D. Ishihara, T. Horie, and M. Denda, J. Exp. Biol. **212**, 1 (2009).
[24] M. Vanella, T. Fitzgerald, S. Preidikman, E. Balaras, and B. Balachandran, J. Exp. Biol. **212**, 95 (2009).
[25] D. Z. Yu, R. W. Mei, and W. Shyy, Int. J. Numer. Methods Fluids **39**, 99 (2002).
[26] Y. Peng, C. Shu, Y. T. Chew, X. D. Niu, and X. Y. Lu, J. Comput. Phys. **218**, 460 (2006).
[27] C. S. Peskin, Ph.D. thesis, Albert Einstein College of Medicine, 1972 (unpublished).
[28] J. Mohd-Yusof, *Annual Research Briefs* (Center for Turbulence Research, Stanford University, Stanford, CA, 1997).
[29] Z. Feng and E. Michaelides, J. Comput. Phys. **202**, 20 (2005).
[30] Y. Peng and L. S. Luo, Prog. Comput. Fluid Dyn. **8**, 156 (2008).
[31] H. Liu and K. Kawachi, J. Comput. Phys. **155**, 223 (1999).
[32] J. Z. Wu, Z. L. Pan, and X. Y. Lu, Phys. Fluids **17**, 098102 (2005).
[33] G. J. Dong, and X. Y. Lu, Phys. Fluids **19**, 057107 (2007).
[34] G. V. Lauder, E. J. Anderson, J. Tangorra, and P. G. Madden, J. Exp. Biol. **210**, 2767 (2007).
[35] J. J. Videler, *Fish Swimming* (Chapman & Hall, London, 1993).
[36] R. Bainbridge, J. Exp. Biol. **35**, 109 (1958).
[37] S. Chen and G. D. Doolen, Annu. Rev. Fluid Mech. **30**, 329 (1998).
[38] Y. Peng, W. Liao, L. S. Luo, and L. P. Wang, Comput. Fluids **39**, 568 (2010).
[39] Y. Liu, N. Liu, and X. Y. Lu, Adv. Appl. Math. Mech. **1**, 481 (2009).
[40] T. Gao and X. Y. Lu, Phys. Fluids **20**, 087101 (2008).
[41] D. d'Humières, Rarefied Gas Dynamics theory and simulations Progress in Astronautics and Aeronautic **159**, 450 (1992).

[42] P. Lallemand and L. S. Luo, Phys. Rev. E **61**, 6546 (2000).
[43] P. Lallemand and L. S. Luo, Phys. Rev. E **63**, 036706 (2003).
[44] J. Zhang, N. S. Liu, and X. Y. Lu, J. Fluid Mech. **659**, 43 (2010).
[45] G. V. Lauder, J. Lim, R. Shelton, C. Witt, E. Anderson, and J. Tangorra, Mar. Tec. Soc. J. **45**, 41 (2011).
[46] L. Shen, X. Zhang, D. K. P. Yue, and M. S. Triantafyllou, J. Fluid. Mech. **484**, 197 (2003).
[47] X. Y. Lu and X. Z. Yin, Acta Mech. **175**, 197 (2005).
[48] J. H. Long, W. Shepherd, and R. G. Root, *Proc. special session on bio-engineering research related to autonomous underwater vehicles, 10th Int. Symp. unmanned untethered submersible technology*, NH, 118–134 (1997).
[49] E. Tytell, C. Y. Hsu, T. L. Williams, A. H. Cohen, and L. J. Fauci, Proc. Natl. Acad. Sci. **107**, 19832 (2010).
[50] G. Dong and X. Y. Lu, Int. J. Numer. Methods Fluids **48**, 1351 (2005).